HAIT Journal of Science and Engineering B, Volume 2, Issues 3-4, pp. 399-425

CHAPTER 2. THEORY, ANALYSIS AND MODELING OF POWER ELECTRONIC CIRCUITS

A novel generalized sampled-data dynamic model for a series-parallel resonant converter under self-sustained oscillation mode. Part I: capacitive output filter

Mohamed Z. Youssef* and Praveen K. Jain

Department of Electrical and Computer Engineering, Queen's University
Walter Light Hall, Kingston, Ontario, Canada K7L 3N6
** Corresponding author: mohamed.youssef@ece.queensu.ca*
Received 1 March 2005, accepted 10 June 2005

Abstract

A novel analytical sampled data dynamic model for a series-parallel resonant converter with capacitive output filter operating in self-sustained oscillation mode (SSOC) is presented. Generalized state-space small-signal and large-signal models, which include the high frequency effects such as leakage inductance of the transformer and series equivalent resistance of the output filter capacitor, are derived for the first time to study the behavior under any loading condition and operating frequency. Finally, numerical solution, simulation results, and experimental results are addressed to verify the proposed methodology. It is shown that the series-parallel converter with capacitive output filter has better transient response than the converter with the inductive-capacitive output filter. The presented modeling technique will be useful in designing the resonant power supplies for low voltage and high current applications with very fast load transient requirement.

1 Introduction

The next decade will force dramatic changes in power supplies. In order to have high speed data-processing chips with lower power consumption, the voltage of power supplies has to go down below 0.5 volts and deliver output currents up to 400 amperes for a single chip with an ultra fast transient response ($> 1000\text{A}/\mu\text{s}$). Isolated resonant DC/DC converters will play a key role in satisfying these requirements. The series-parallel resonant converter is a good candidate for achieving these features. The fast dynamic response can be significantly improved by using a capacitive filter in the output. The resonant converter should have an accurate analysis as a mandatory requirement for a sound design procedure. In this paper, the modeling and analysis of the series-parallel resonant converter with a capacitive output filter using the sampled-data theory is presented. This modeling is presented in a closed loop form with the converter equipped with the self-sustained oscillation controller (SSOC) [1]. This modeling procedure should lead to a successful design of the converter that meets the anticipated performance features. These features are: zero-voltage-switching (ZVS) down from full load to no load, acceptable overall working efficiency, significant reduction in the frequency variation range needed for ZVS to guarantee size compactness, and an ultra-fast transient response.

A number of attempts was made to attain a speedy transient performance by modifying the principle of operation of existing topologies through adding auxiliary circuits, which increase the number of components and the conduction losses deteriorating the efficiency [2-6]. Other tried to get new control topologies capable of providing a higher bandwidth by modifying existing control configurations, which got the control loop crowded with components affecting its long-term reliability. In addition, all of their modeling suffers tough mathematical computation [2-10]. The proposed converter with the SSOC has the capabilities to heal all of the above disadvantages. In order to understand its operation well, an accurate mathematical model must be derived. The converter employs the sampled-data theory to obtain a versatile dynamic model capable of emulating the steady state, large signal, and small signal responses accurately. This sampled data model provides a systematic procedure to study the converter dynamics, avoiding the previous continuous time models complexity [11]. This paper is organized as follows: part II will explain the applicability of the self-sustained oscillation (SSOC) topology to the proposed converter, in part III the derivation of dynamic model is investigated, in part IV analytical, simulation, and experimental

results for a design case are studied. Finally, conclusions of the originality of the proposed work are illustrated.

2 Generalization of the self-sustained oscillation for the series-parallel resonant converter with capacitive output filter

Let us consider the series-parallel resonant converter with capacitive output filter of Fig. 1. In order to derive the sampled-data model for this converter, it is necessary to consider the events that characterize the transition between the circuit configurations. For the converter of Fig. 1 these events are:

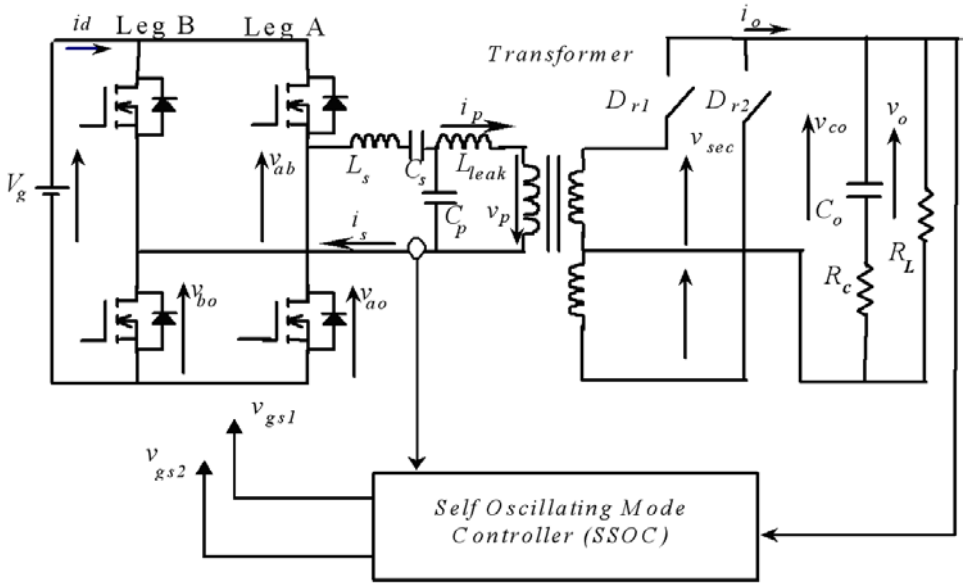

Figure 1: Full bridge series-parallel resonant dc-dc converter with capacitive output filter.

1. the turning on of the output rectifiers when the voltage (v_{cp}) is greater than (v_o),
2. the turning off of the output rectifiers when the current (i_s) crosses zero,
3. the trailing edge of the voltage (v_{ab}) when the control signal (v_{ca}) becomes greater than the saw-tooth signal (s_t),
4. the leading edge of the voltage (v_{ab}) when the current (i_s) crosses zero.

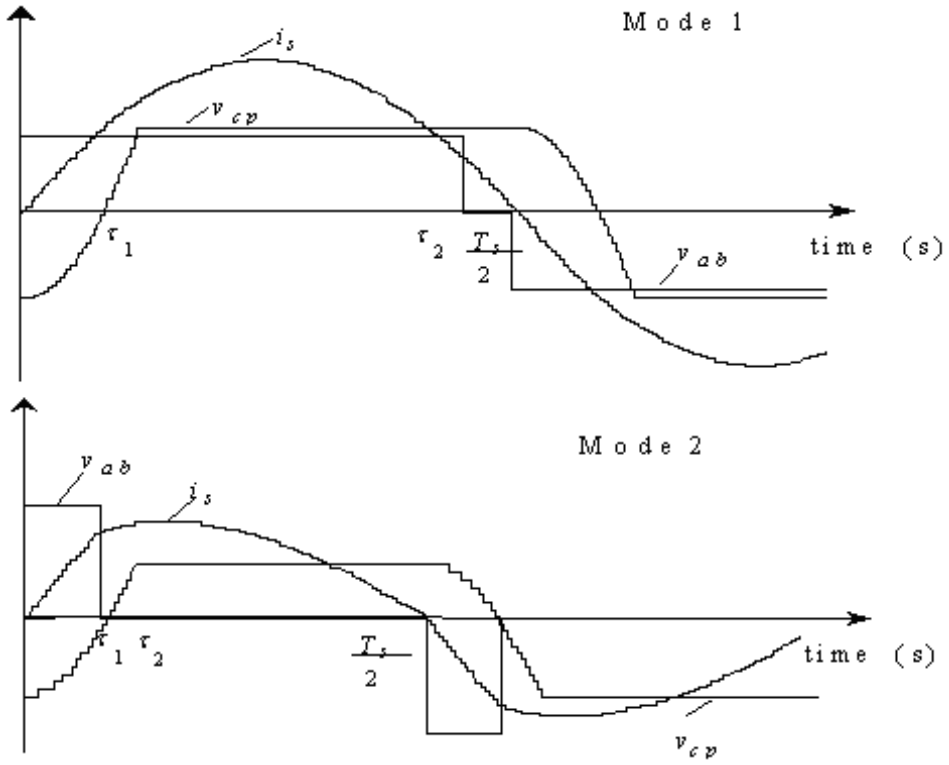

Figure 2: Modes of operation.

By assuming that the current (i_s) crosses zero at t=0, only the events (a) and (c) occur within the rest of the semi-cycle. As a result, two modes of operation exist depending on the order of these events within the semi-cycle, as shown in Fig. 2. Knowing boundary conditions, exact sampled-data models for both modes can be derived and used to obtain the main characteristics of the converter.

Before proceeding with the mathematical modeling, it is worth to define the following basic quantities.

(i) Base time $=\sqrt{L_S C_S} = \frac{1}{\omega_o}$, (ii) base voltage = V_g = rated input voltage, (iii) base current $=V_g \Big/ \sqrt{L_S/C_S}$. With these base quantitiesand assuming the unit transformer ratio, we find the following state-space representation for Mode 1 when the event (1) occurs before the event (3):

$$\begin{bmatrix} \frac{di_s'}{dt'} \\ \frac{dv_s'}{dt'} \\ \frac{dv_{cp}}{dt'} \\ \frac{di_p'}{dt'} \\ \frac{dv_{co}}{dt'} \\ \frac{dx_s}{dt'} \\ \frac{ds_t}{dt'} \end{bmatrix} = \begin{bmatrix} 0 & -1 & -1 & 0 & 0 & 0 & 0 \\ 1 & 0 & 0 & 0 & 0 & 0 & 0 \\ \beta & 0 & 0 & -\beta & 0 & 0 & 0 \\ 0 & \frac{1-\varpi_0}{\varpi_0} & \frac{1-\varpi_0}{\varpi_0} & 0 & 0 & 0 & 0 \\ 0 & 0 & 0 & \frac{c_S}{c_0(1+\frac{R_C}{R_L})} & \frac{-\sqrt{\frac{L_S}{C_S}}}{R_L(1+\frac{R_C}{R_L})} & 0 & 0 \\ 0 & 0 & 0 & 0 & 0 & 0 & \frac{-K_{p_1}}{\omega_o} \\ 0 & 0 & 0 & 0 & 0 & \frac{K_{p_2}}{\omega_o} & 0 \end{bmatrix}$$
$$\cdot \begin{bmatrix} i_s' \\ v_s' \\ v_{cp}' \\ i_p' \\ v_{co}' \\ x_s \\ s_t \end{bmatrix} + \begin{bmatrix} 1 & 0 \\ 0 & 0 \\ 0 & 0 \\ (1-\frac{1}{\omega_o}) & 0 \\ 0 & 0 \\ 0 & \frac{k_{p_1}}{2\omega_o} \\ 0 & 0 \end{bmatrix} \begin{bmatrix} V' \\ V_P \end{bmatrix} \qquad (1)$$

where the symbol ($\prime$) is used to denote normalized quantities. Note that the states of the SSOC, x_s and s_t for the controller model are given in the Appendix. Similarly, the state space equation that represents the converter in Mode 2 is:

$$\begin{bmatrix} \frac{di_s^{'}}{dt^{'}} \\ \frac{dv_s^{'}}{dt^{'}} \\ \frac{dv_{cp}^{'}}{dt^{'}} \\ \frac{di_p^{'}}{dt^{'}} \\ \frac{dv_{co}^{'}}{dt^{'}} \\ \frac{dx_s}{dt^{'}} \\ \frac{ds_t}{dt^{'}} \end{bmatrix} = \begin{bmatrix} 0 & -1 & -1 & 0 & 0 & 0 & 0 \\ 1 & 0 & 0 & 0 & 0 & 0 & 0 \\ \beta & 0 & 0 & -\beta & 0 & 0 & 0 \\ 0 & 0 & \beta' & 0 & 0 & 0 & 0 \\ 0 & 0 & 0 & 0 & \frac{-\sqrt{\frac{L_S}{C_S}}}{R_L(1+\frac{R_C}{R_L})} & 0 & 0 \\ 0 & 0 & 0 & 0 & 0 & 0 & \frac{-K_{p1}}{\omega_o} \\ 0 & 0 & 0 & 0 & 0 & \frac{K_{p2}}{\omega_o} & 0 \end{bmatrix}$$

$$\cdot \begin{bmatrix} i_s^{'} \\ v_s^{'} \\ v_{cp}^{'} \\ i_p^{'} \\ v_{co} \\ x_s \\ s_t \end{bmatrix} + \begin{bmatrix} 1 & 0 \\ 0 & 0 \\ 0 & 0 \\ 0 & 0 \\ 0 & 0 \\ 0 & \frac{k_{p1}}{2\omega_o} \\ 0 & 0 \end{bmatrix} \begin{bmatrix} V^{'} \\ V_P \end{bmatrix}. \tag{2}$$

The solution of the state space equations (1) and (2) for Modes 1 and 2 can be expressed as:

$$\begin{bmatrix} i_s^{'}(t^{'}) \\ v_s^{'}(t^{'}) \\ v_{cp}^{'}(t^{'}) \\ i_p^{'}(t^{'}) \\ v_{co}(t^{'}) \\ x_s(t') \\ s_t(t') \end{bmatrix} = \phi_1(t'-t'_o) \begin{bmatrix} i_s^{'}(t_o^{'}) \\ v_s^{'}(t_o^{'}) \\ v_{cp}^{'}(t_o^{'}) \\ i_p^{'}(t_o^{'}) \\ v_{co}(t_o^{'}) \\ x_s(t_o^{'}) \\ s_t(t_o^{'}) \end{bmatrix} + \psi_1(t'-t'_o) \begin{bmatrix} V^{'} \\ V_P \end{bmatrix} \tag{3}$$

$$\begin{bmatrix} i_s^{'}(t^{'}) \\ v_s^{'}(t^{'}) \\ v_{cp}^{'}(t^{'}) \\ i_p^{'}(t^{'}) \\ v_{co}(t^{'}) \\ x_s(t') \\ s_t(t') \end{bmatrix} = \phi_2(t'-t'_o) \begin{bmatrix} i_s^{'}(t_o^{'}) \\ v_s^{'}(t_o^{'}) \\ v_{cp}^{'}(t_o^{'}) \\ i_p^{'}(t_o^{'}) \\ v_{co}(t_o^{'}) \\ x_s(t_o^{'}) \\ s_t(t_o^{'}) \end{bmatrix} + \psi_2(t'-t'_o) \begin{bmatrix} V^{'} \\ V_P \end{bmatrix} \tag{4}$$

where the expositional state transition matrix $\phi_1(.)$, its integral transition matrix $\Psi_1(.)$, as well as $\phi_2(.)$ with its expositional integral transition matrix $\Psi_2(.)$ are:

$$\phi_1(\tau) = \begin{bmatrix} \cos\sqrt{(1+\beta)}\tau) & -\frac{\sin(\sqrt{(1+\beta)}\tau)}{\sqrt{(1+\beta)}} & -\frac{\sin(\sqrt{(1+\beta)}\tau)}{\sqrt{(1+\beta)}} & 2\cos\sqrt{(1+\beta)}\tau) & 0 & 0 & 0 \\ \frac{\sin(\sqrt{(1+\beta)}\tau)}{\sqrt{(1+\beta)}} & \frac{\beta+\cos(\sqrt{(1+\beta)}\tau)}{\sqrt{(1+\beta)}} & \frac{-1+\cos(\sqrt{(1+\beta)}\tau)}{\sqrt{(1+\beta)}} & 2\frac{\sin(\sqrt{(1+\beta)}\tau)}{\sqrt{(1+\beta)}} & 0 & 0 & 0 \\ \frac{\beta\sin(\sqrt{(1+\beta)}\tau)}{\sqrt{(1+\beta)}} & \frac{-\beta+\beta\cos(\sqrt{(1+\beta)}\tau)}{\sqrt{(1+\beta)}} & \frac{1+\beta\cos(\sqrt{(1+\beta)}\tau)}{\sqrt{(1+\beta)}} & 2\frac{\beta\sin(\sqrt{(1+\beta)}\tau)}{\sqrt{(1+\beta)}} & 0 & 0 & 0 \\ -\cos(\sqrt{(1+\beta)}\tau) & \frac{\sin(\sqrt{(1+\beta)}\tau)}{\sqrt{(1+\beta)}} & \frac{\sin(\sqrt{(1+\beta)}\tau)}{\sqrt{(1+\beta)}} & \sin(\sqrt{(1+\beta)}\tau) & 0 & 0 & 0 \\ 0 & 0 & 0 & 1 & -1 & 0 & 0 \\ 0 & 0 & 0 & 0 & 0 & \cos(\upsilon\tau) & -\frac{\upsilon\omega_o\sin(\omega_o\tau)}{k_{p_2}} \\ 0 & 0 & 0 & 0 & 0 & \frac{\upsilon\omega_o\sin(\omega_o\tau)}{k_{p_1}} & \cos(\upsilon\tau) \end{bmatrix} \tag{5}$$

$$\psi_1(\tau) = \begin{bmatrix} \frac{\sin\sqrt{(1+\beta)}\tau}{\sqrt{(1+\beta)}} & 0 \\ \frac{1-\cos\sqrt{(1+\beta)}\tau}{(1+\beta)} & 0 \\ \frac{\beta(1-\cos\sqrt{(1+\beta)}\tau)}{(1+\beta)} & 0 \\ 2\frac{\sin\sqrt{(1+\beta)}\tau}{\sqrt{(1+\beta)}} & 0 \\ 0 & 0 \\ 0 & \frac{k_{p_1}\sin(\upsilon\tau)}{\upsilon\omega_o} \\ 0 & 1-\cos(\upsilon\tau) \end{bmatrix} \tag{6}$$

$$\phi_2(\tau) = \begin{bmatrix} \cos(\tau) & -\sin(\tau) & -1 & 2\cos(\tau) & 0 & 0 & 0 \\ \sin(\tau) & \cos(\tau) & -1 & 2\sin(\tau) & 0 & 0 & 0 \\ 1 & 0 & 0 & -1 & 0 & 0 & 0 \\ 0 & 0 & -1 & 0 & 0 & 0 & 0 \\ 0 & 0 & 0 & 0 & 1 & 0 & 0 \\ 0 & 0 & 0 & 0 & 0 & \cos(\upsilon\tau) & -\frac{\upsilon\omega_o\sin(\omega_o\tau)}{k_{p_2}} \\ 0 & 0 & 0 & 0 & 0 & \frac{\upsilon\omega_o\sin(\omega_o\tau)}{k_{p_1}} & \cos(\upsilon\tau) \end{bmatrix} \tag{7}$$

$$\psi_2(\tau) = \begin{bmatrix} \sin(\tau) & 0 \\ 1-\cos(\tau) & 0 \\ \beta(1-\cos(\tau) & 0 \\ \tau & 0 \\ 0 & 0 \\ 0 & \frac{k_{p_1}\sin(\upsilon\tau)}{\upsilon\omega_o} \\ 0 & 1-\cos(\upsilon\tau) \end{bmatrix} \tag{8}$$

where $\beta = C_s/C_p$ is the ratio of the series and parallel capacitors, $\beta\prime = L_s/L_{leak}$ is the ratio between the resonant tank inductance and the transformer leakage inductance, the base frequency (rad/sec.) $\omega_o = {}^{1}/_{\sqrt{L_sC_s}}$, the base time $\tau_o = \frac{1}{\omega_o}$, (ν) is the ratio between the control saw-tooth frequency (ω_{st}) and the resonant frequency,$\omega_{st} = \sqrt{k_{p_1}k_{p_2}}$, (R_c) is the equivalent series resistance of the output filter capacitance, (i'_p) is the normalized transformer primary current passing through the leakage inductance, (v'_{co}) is the normalized voltage across the output filter capacitor, and (R_L) is the load resistance.

3 Derivation of dynamic models

3.1 Large signal model

Let us consider that the series-parallel resonant converter operates cyclically with a succession of linear time invariant circuit configurations in each cycle. This can be described by a non-linear sampled-data model:

$$x_{k+1} = f(x_k, u_k), \tag{9}$$

$$\sigma(x_k, u_k) = 0. \tag{10}$$

The components of the vector x_k are the variables of the converter sampled at the moment when the current i_s crosses zero, and are given by $x_k = [i'_s(t_k) \quad v'_s(t_k) \quad v'_{cp}(t_k) \quad i'_p(t_k)\ v'_{co}(t_k) \quad x_s(t_k) \quad s_t(t_k)]^T$. On the other hand, the input vector $\boldsymbol{u}_k$ is comprised of two vectors, $\boldsymbol{u}_k = [\ \boldsymbol{p}_k,\ \boldsymbol{w}_k]$. The components of the vector $\boldsymbol{w}_k$ are the transition times, defined as $\boldsymbol{w}_k = [\tau_1\ \tau_2]^T$. Finally, the vector $\boldsymbol{p}_k$ contains the input sources of the circuit, that is, $\boldsymbol{p}_k = [v'_g \quad V_p]^T$. The function $\boldsymbol{f}(.)$ for Mode 1 is:

$$
\begin{aligned}
f(x_k, u_k) &= \phi_2(\frac{T_s}{2} - \tau_2) \\
&\cdot\phi_2(\tau_2 - \tau_1)\left[(\Phi_1(\tau_1)\Phi_0 W x_k + \Psi_1(\tau_1) I_1 p_k\right] + \psi_2(\tau_2 - \tau_1) I_1 p_k \\
&+\psi_2(\frac{T_s}{2} - \tau_2) I_2 p_k.
\end{aligned} \tag{11}
$$

However, the matrix (ϕ_o) is defined to represent the reset pulse (RP), which allows the saw-tooth signal to be reset whenever the current (i_s) crosses zero, described as:

$$
\phi_o = \begin{bmatrix}
1 & 0 & 0 & 0 & 0 & 0 & 0 \\
0 & 1 & 0 & 0 & 0 & 0 & 0 \\
0 & 0 & 1 & 0 & 0 & 0 & 0 \\
0 & 0 & 0 & 1 & 0 & 0 & 0 \\
0 & 0 & 0 & 0 & 1 & 0 & 0 \\
0 & 0 & 0 & 0 & 0 & 1 & 0 \\
0 & 0 & 0 & 0 & 0 & 0 & 0
\end{bmatrix}. \tag{12}
$$

Finally, the matrix (W) is used to exploit the half-wave symmetry of the resonant circuit variables and given by:

$$
W = \begin{bmatrix}
-1 & 0 & 0 & 0 & 0 & 0 & 0 \\
0 & -1 & 0 & 0 & 0 & 0 & 0 \\
0 & 0 & -1 & 0 & 0 & 0 & 0 \\
0 & 0 & 0 & -1 & 0 & 0 & 0 \\
0 & 0 & 0 & 0 & 1 & 0 & 0 \\
0 & 0 & 0 & 0 & 0 & 1 & 0 \\
0 & 0 & 0 & 0 & 0 & 0 & 1
\end{bmatrix}. \tag{13}
$$

The matrices (I1) and (I2) are introduced to adjust the half-wave symmetry analysis of the circuit:

$$
I_1 = \begin{bmatrix} 1 & 0 \\ 0 & 1 \end{bmatrix} \quad I_2 = \begin{bmatrix} 0 & 0 \\ 0 & -1 \end{bmatrix}. \tag{14}
$$

On the other hand, the entries of the vector function $\boldsymbol{\sigma}(.)$ are constraint equations related with the event that characterizes the end of each circuit configuration. For Mode 1 of operation the vector function $\sigma(.)$ is given by:

$$\sigma(x_k, u_k) = \begin{bmatrix} \sigma_{11} \\ \sigma_{21} \\ \sigma_{31} \end{bmatrix}$$

$$\sigma_{11} = [\phi_1(\tau_1)\phi_o w x_k + \psi_1(\tau_1) I_1 p_k]_3 - v_o$$

$$\sigma_{21} = \phi_2(\tau_2 - \tau_1)\left[\phi_1(\tau_1)\phi_o w x_k + \psi_1(\tau_1) I_1 p_k\right] + \psi_2(\tau_2 - \tau_1) I_1 p_k]_5 - v_{ca}$$

$$\sigma_{31} = \begin{bmatrix} \phi_2(\frac{T_s}{2} - \tau_2) \\ \cdot\{\phi_2(\tau_2 - \tau_1)\left[\phi_1(\tau_1)\phi_o w x_k + \psi_1(\tau_1) I_1 p_k\right] + \psi_2(\tau_2 - \tau_1) I_1 p_k\} \\ +\psi_2(\frac{T_s}{2} - \tau_2) I_2 p_k \end{bmatrix}_1, \tag{15}$$

for Mode 2 of operation the functions $\boldsymbol{f}(.)$ and $\sigma(.)$ are :

$$\begin{aligned} f(x_k, u_k) \quad = \quad & \phi_2(\frac{T_s}{2} - \tau_2) \\ & \cdot\{\phi_2(\tau_2 - \tau_1)\left[(\Phi_1(\tau_1)\Phi_0 W x_k + \Psi_1(\tau_1) I_1 p_k\right] + \psi_2(\tau_2 - \tau_1) I_2 p_k\} \\ & +\psi_2(\frac{T_s}{2} - \tau_2) I_2 p_k. \end{aligned} \tag{16}$$

$$\sigma(x_k, u_k) = \begin{bmatrix} \sigma_{11} \\ \sigma_{21} \\ \sigma_{31} \end{bmatrix}$$

$$\sigma_{11} = [\phi_1(\tau_1)\phi_o w x_k + \psi_1(\tau_1) I_1 p_k]_5 - v_{ca}$$

$$\sigma_{21} = \phi_2(\tau_2 - \tau_1)\left[\phi(\tau_1)\phi_o w x_k + \psi_1(\tau_1) I_1 p_k\right] + \psi_2(\tau_2 - \tau_1) I_2 p_k]_3 - v_o$$

$$\sigma_{31} = \begin{bmatrix} \phi_2(\frac{T_s}{2} - \tau_2) \\ \cdot\{\phi_2(\tau_2 - \tau_1)\left[\phi_1(\tau_1)\phi_o w x_k + \psi_1(\tau_1) I_1 p_k\right] + \psi_2(\tau_2 - \tau_1) I_1 p_k\} \\ +\psi_2(\frac{T_s}{2} - \tau_2) I_2 p_k \end{bmatrix}_1. \tag{17}$$

For Mode 1, after some manipulations using equations (9), (10), (11), and (15) we can find that the time constants τ_1 and τ_2 must satisfy the relation:

$$V_o = \left\{ \begin{array}{l} [\varphi_1(\tau_1)\varphi_o w[\varphi_2(\frac{\tau_s}{2}-\tau_2)\varphi_2(\tau_2-\tau_1)\varphi_1(\tau_1)\varphi_o w]^{-1} \\ \\ [\varphi_2(\frac{\tau_s}{2}-\tau_2)\varphi_2(\tau_2-\tau_1)\psi_1(\tau_1)I_1+\psi_2(\frac{\tau_s}{2}-\tau_2)I_2]+\psi_1(\tau_1)I_1] \end{array} \right\}_3 . \quad (18)$$

3.2 Static characteristics for operation with self-sustained oscillation

The boundary between the Modes 1 and 2 of operation in the circuit parameter space can be found by solving (11) (15), (16), and (17) to find a steady-state solution with $0<\tau_1=\tau_2<T_s/2$. Figs. 3 to 6 will be the guideline for the design of the converter parameters through the selection of the minimum possible quality factor (Q_s) along with a sufficient voltage ratio required for ZVS.

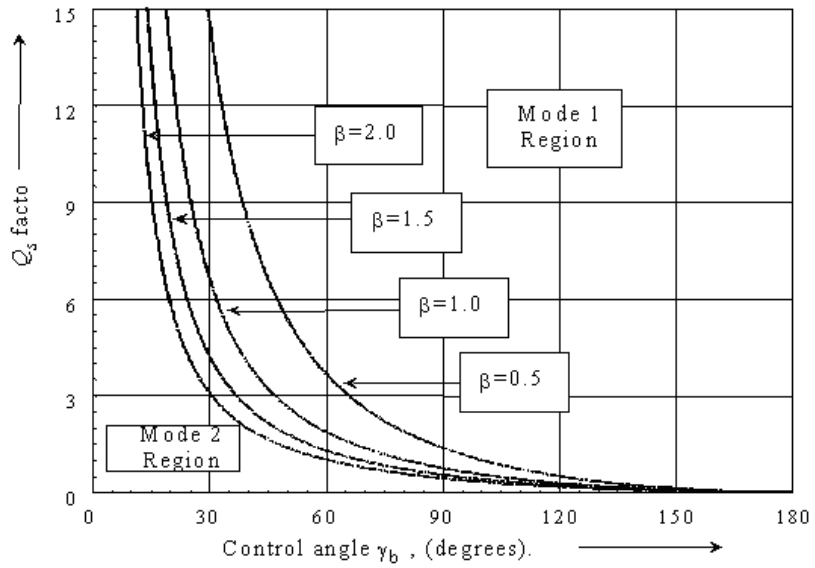

Figure 3: Boundaries between the modes of operation.

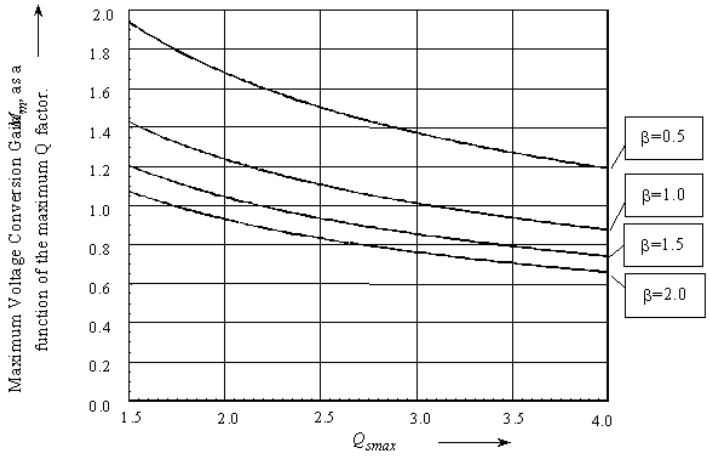

Figure 4: Maximum voltage conversion ratio for operation at constant output voltage with a capacitive filter.

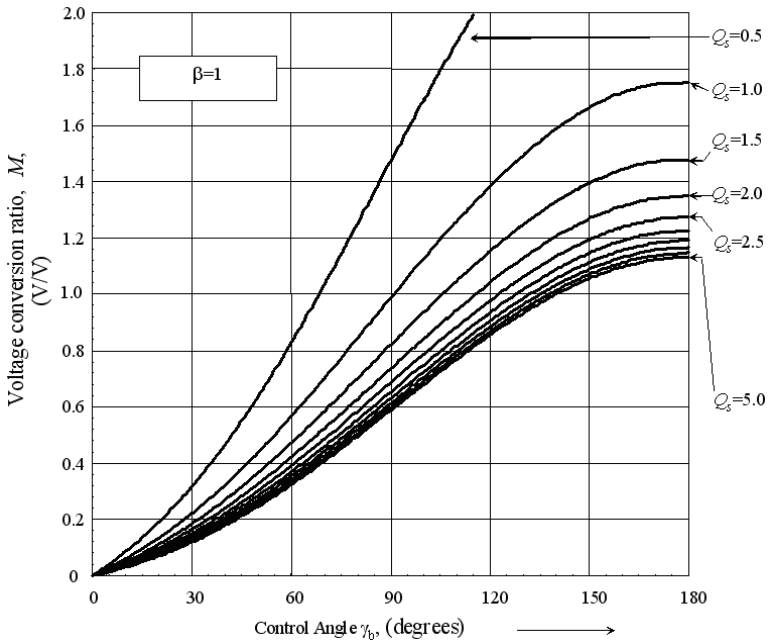

Figure 5: Voltage conversion ratio as a function of the control angle γ_b.

Figure 4 shows the relation between the voltage conversion ratio (M) and the maximum quality factor (Q_s) for different values of (β). The choice of a reasonable value around ($Q_s = 1.5$) and (β=1) will guarantee the voltage ratio of (1.44), which is fairly sufficient to achieve ZVS [Appendix].

Figure 5 shows the variation of the control angle (γ_b) with the voltage ratio (M) at different quality factors. The best quality factor that guarantees a voltage ratio sufficient to achieve ZVS with minimum stress on the tank elements is around (1.5).

Figure 6 shows that the corresponding switching frequency ratio for ($Q_s = 1.5$) and (β=1) is around (1.14), lower than the value (1.44) needed for the conventional variable frequency control, which is a merit for the SSOC methodology.

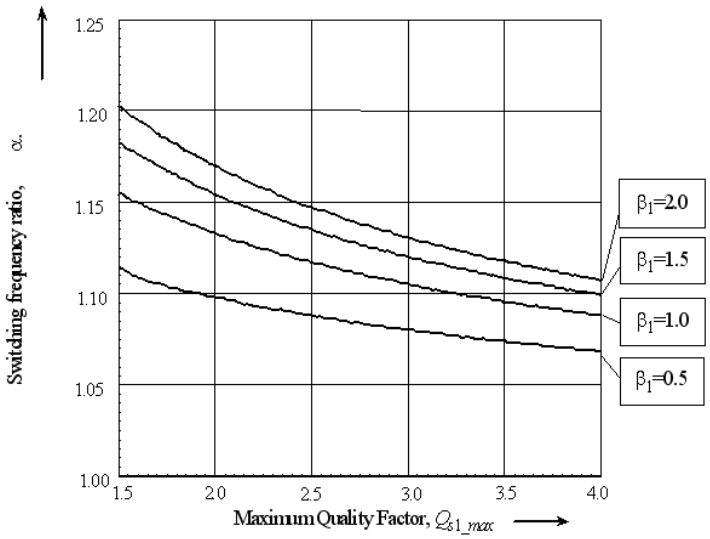

Figure 6: Switching frequency ratio with a capacitive output filter.

3.3 Small signal model

In order to derive the small signal model, we must solve the following set of equations:

$$\begin{aligned} x_{k+1} &= x_k, \\ \sigma(x_k, u_k) &= 0, \end{aligned} \tag{19}$$

then, by linearizing the nonlinear sampled model around a given point, this linear time invariant model can be expressed using the form:

$$x_{k+1} = Ax_k + Bu_k. \tag{20}$$

However, the state matrix A can be given as:

$$\begin{aligned} A &= \frac{\partial f}{\partial x} - \frac{\partial f}{\partial w}[\frac{\partial \sigma}{\partial w}]^{-1}\frac{\partial \sigma}{\partial x} \\ A &= \phi_2(\tfrac{\tau_s}{2} - \tau_2)\phi_1(\tau_2 - \tau_1)\phi_1(\tau_1)\phi_O w. \end{aligned} \tag{21}$$

Also, the input matrix B is described by:

$$\begin{aligned} B &= \frac{\partial f}{\partial p} - \frac{\partial f}{\partial w}[\frac{\partial \sigma}{\partial w}]^{-1}\frac{\partial \sigma}{\partial p} \\ B &= \phi_2(\tfrac{\tau_s}{2} - \tau_2)\phi_2(\tau_2 - \tau_1)\psi_1(\tau_1)I_1 + \psi_2(\tau_2 - \tau_1)I_1 + \psi_2(\tfrac{\tau_s}{2} - \tau_2)I_2. \end{aligned} \tag{22}$$

In solution of these equations, the non-linear sampled data model can be expressed as a linear time invariant model for small perturbations around the operating point. In order to determine (τ_1) and (τ_2) to get the state space matrices, the following procedure is suggested:

1. define M, and β;
2. from the static characteristics (Figs. 3 to 6), get the (Q_s), switching frequency (T_s), and the required (γ_b);
3. through (γ_b), get (τ_2);
4. using equation (18), get (τ_1);
5. build the state space matrices suitable for any small perturbation stability test.

4 Simulation and experimental results

4.1 Output filter dynamic response

Normally, the output filter attenuates the low frequency oscillation of the dc output voltage in addition to the high frequency components of the output current. The second-order ***LC*** filter results from a trade-off between the elimination of output current ripple and the inhibition of the transient

response due to its inductance. However, the capacitive filter can attain a faster transient response with a reasonable capacitor value, according to recent achievements in capacitor design. Two prototypes were made, the first with an inductive output filter, then the other with a capacitive filter for performance comparison. The parameters of the two converters working at 100 kHz and power of 1 kW with input and output voltages of 250 and 100 V, respectively, are tabulated below.

L_s	C_s	C_p	$n_1 : n_2$	L_o	C_o	$L_{leakage}$	$ESR\ of\ C_o$
$208\mu H$	$15.8nF$	$15.8nF$	2.29	$10\mu H$	$22\mu F$	$1\mu H$	$1m\Omega$

Table 1: Converter with an inductive output filter.

L_s	C_s	C_p	$n_1 : n_2$	C_o	$L_{leakage}$	$ESR\ of\ C_o$
$55\mu H$	$60nF$	$41nF$	13 : 11	$220\mu F$	$1\mu H$	$7.5m\Omega$

Table 2: Converter with a capacitive output filter.

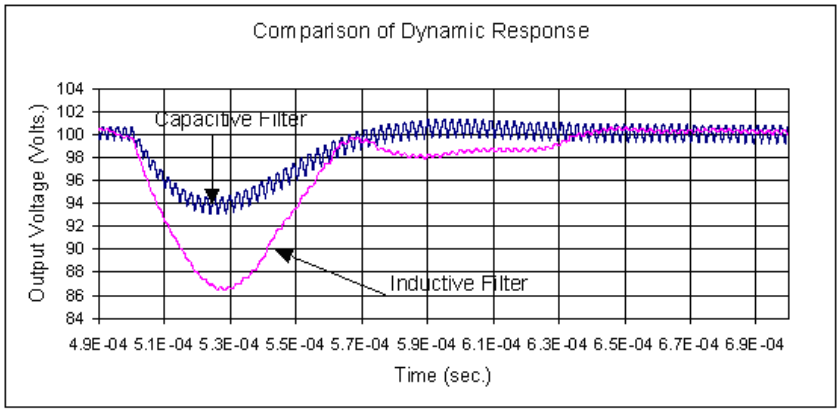

Figure 7: Simulation results: comparison of transient responses for capacitive and inductive filters.

The simulation results in Figs. 7 and 8 show that the capacitive filter is capable of delivering a faster dynamic response than that of the LC filter. Fig. 7 shows that the converter with an inductive output filter suffers a larger voltage dip for a step disturbance in the output current than that equipped with a capacitive output filter. Fig. 8 shows that the capacitive

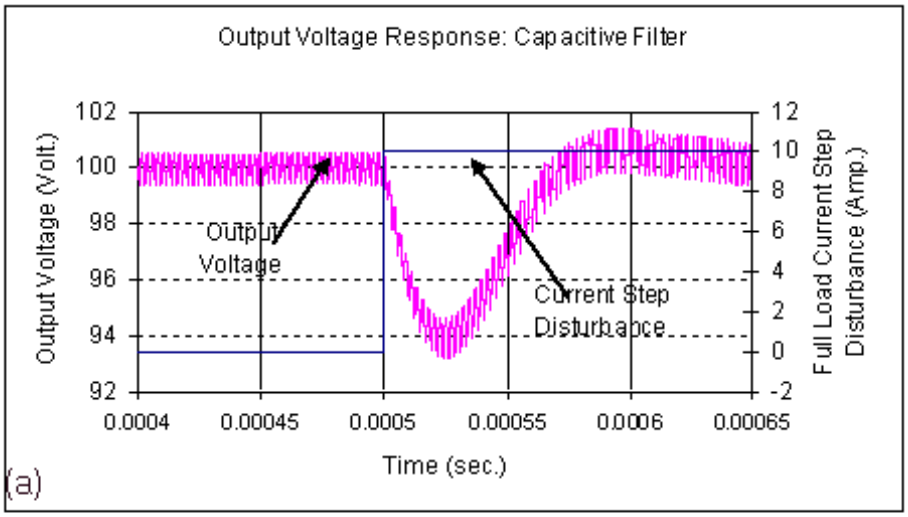

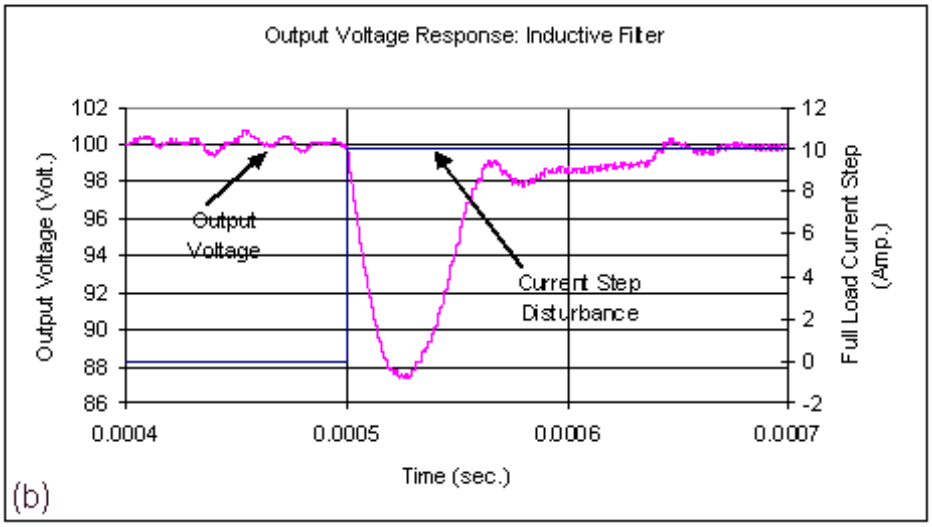

Figure 8: Simulation results for a capacitive (a) and inductive (b) filters: full load current (150A/μs) step disturbance shows the robustness of the converter output voltage with capacitive filter.

output filter converter has a faster transient response in restoring the output voltage value with a considerably smaller voltage dip. Consequently, these features can introduce the proposed converter with capacitive output filter to be a good candidate for low voltage high current applications since it has a fast transient response and lower overshoot standing for a reasonable value of load current slew rate (150A/μsec).

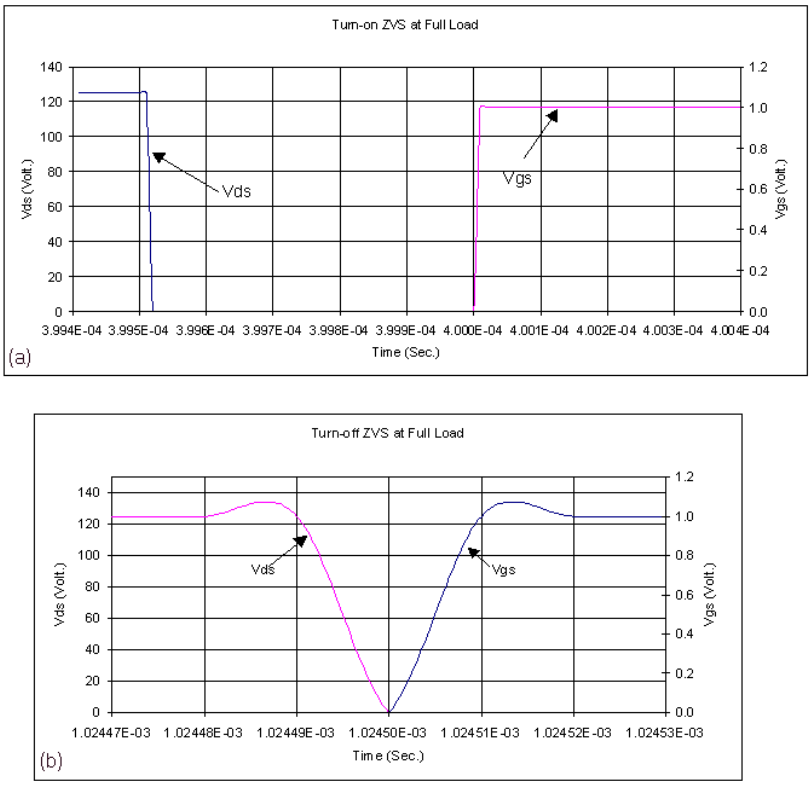

Figure 9: PSIM simulation results: ZVS at full load operation: (a) full load ZVS turn-on, (b) full load ZVS turn-off.

4.2 ZVS illustration

Simulation in different operating conditions was investigated to assure the ZVS existence for the proposed converter as shown in Fig. 10. It shows that the gate-source voltage and the drain-source voltage are acting in an opposite manner, so that none of them is initiated unless the other is completely

brought to zero. As a result, the converter enjoys the ZVS at both turn-off and turn-on in different situations at full load and half load.

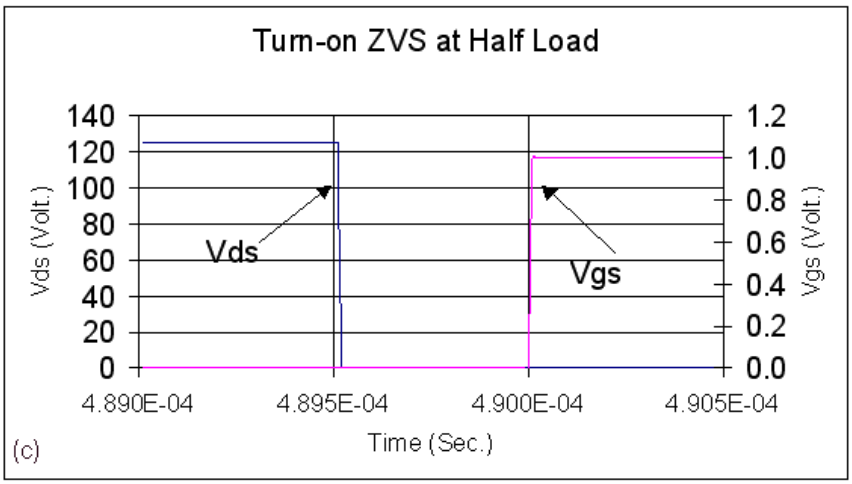

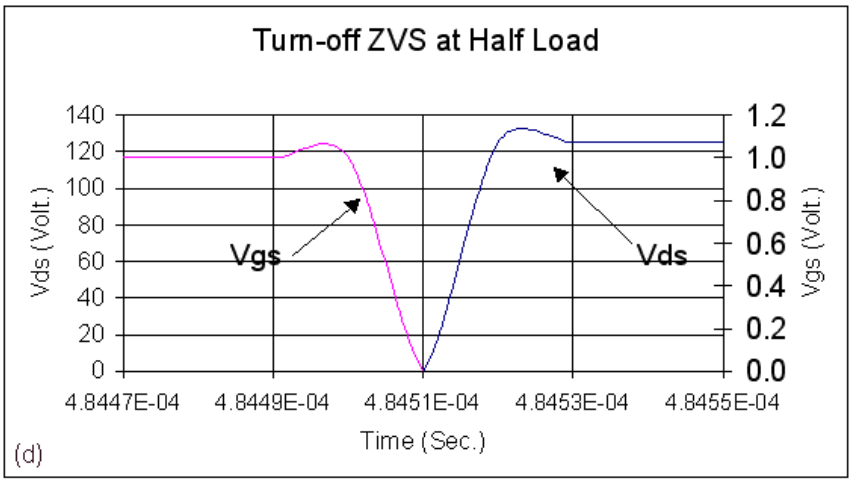

Figure 10: PSIM simulation results: ZVS at half load operation: (c) turn-on ZVS at half load, (d) half load turn-off ZVS.

Experimentally, the ZVS was tested over the loading range, which includes short-circuit, full-load, and no-load, with the results shown in Fig 11. It is possible to see that at any of the aforementioned operating conditions the drain-source voltage is already zero before the gate-source voltage becomes high; in addition the resonant tank current has a phase lag with respect to the inverter output voltage indicating the right polarity to discharge snubber capacitors of the switches, necessary to achieve ZVS.

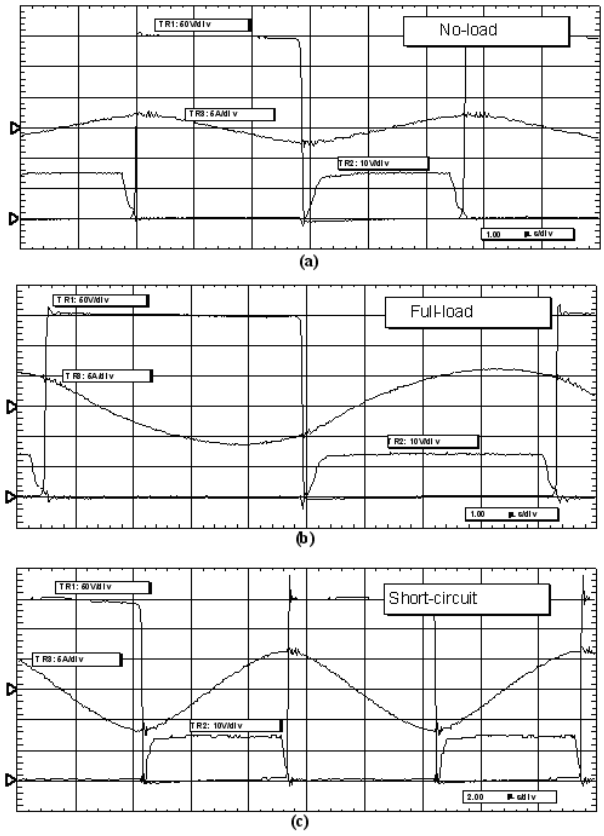

Figure 11: Experimental results showing zero voltage switching during (a) no-load, (b) full-load, and (c) short-circuit. TR1 is the voltage across the leg B of the inverter v_{bo}or, in other words, v_{ds2} TR2 is the gate to source voltage of the Leg B bottom transistor (v_{gs2}), TR3 is the current through the series resonant inductor i_s.

4.3 Performance evaluation

The capacitive output filter is capable not only to provide zero voltage switching and faster transient response but also an acceptable overall efficiency during the whole working range from light loads up to full load, as shown in Fig. 12.

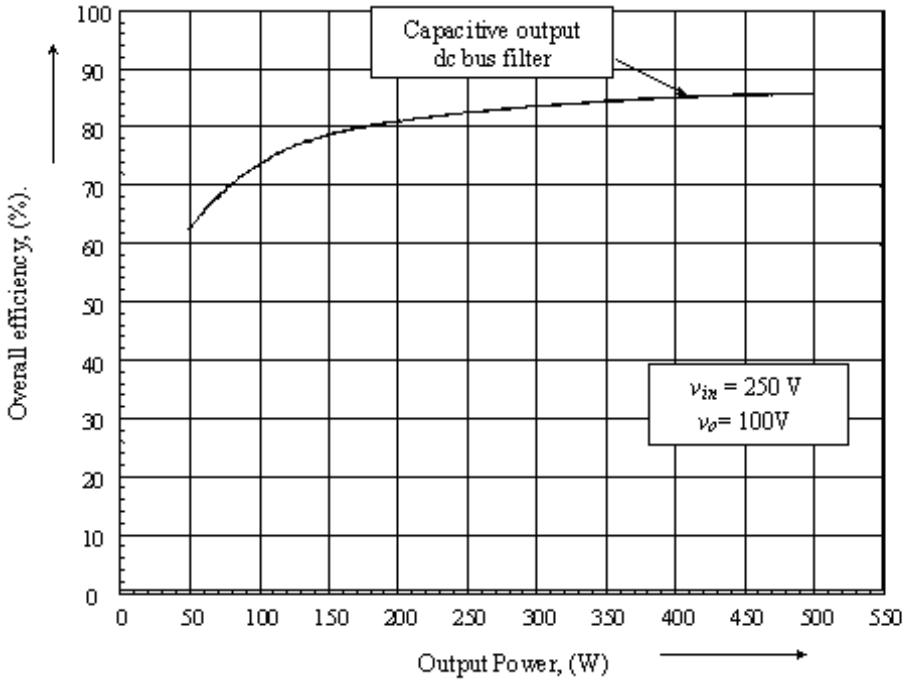

Figure 12: Experimental results: overall efficiency variation with the load.

4.4 Dynamic model stability

Using the small signal model developed, the stability of the proposed converter with a capacitive filter was tested under a step disturbance in the control angle from 115 $^{\circ}$ to 125 $^{\circ}$. The root loci of the sampled data model shows that the eigenvalues change such that they are always within the unit circle indicating stability. In addition, the damping ratio provided is 0.75, showing good robustness.

Eigenvalues before disturbance	Eigenvalues after disturbance
0.0002	0.0001
0.0005	0.0003
$0.0788 + 0.0897i$	$0.0541 + 0.0757i$
$0.0788 - 0.0897i$	$0.0541 - 0.0757i$
0.0029	0.0019
-0.0001	0.00008
0.0011	0.0005

Table (3): Eigenvalues of the system.

The frequency bode plot is shown in order to prove the seventh order presentation as the phase ends at 630°, the crossover frequency is at (–20db/decade) to ensure a satisfactory phase margin, and the gain at higher frequencies is very low in order to attenuate noise at these frequencies. In addition, it has a fairly reasonable gain at low frequencies to reduce the steady state error. Finally, the converter has the capabilities to meet satisfactory control specifications.

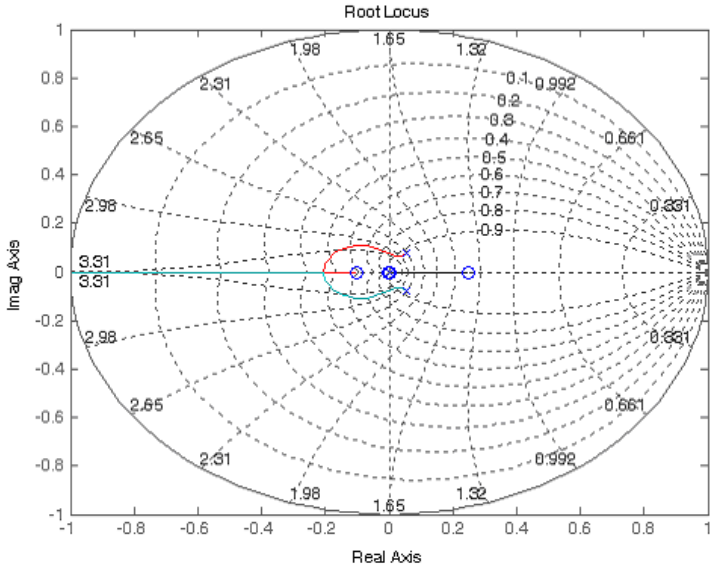

Figure 13: Root loci of the system after disturbance.

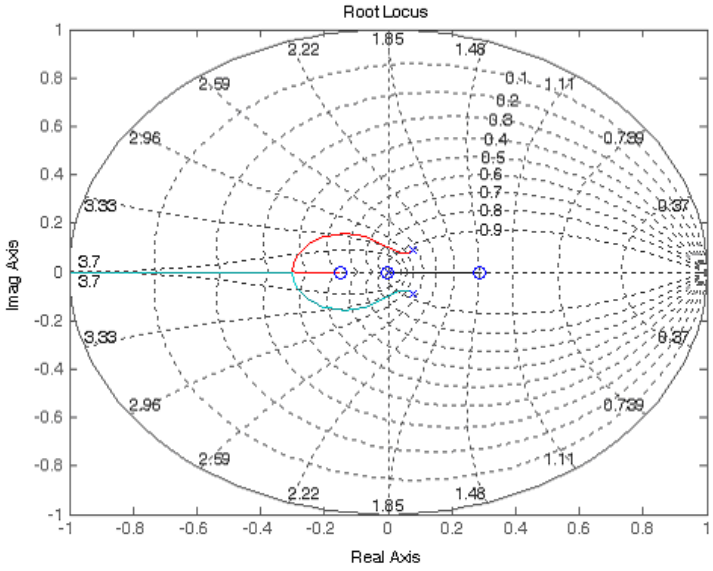

Figure 14: Root loci of the system before disturbance.

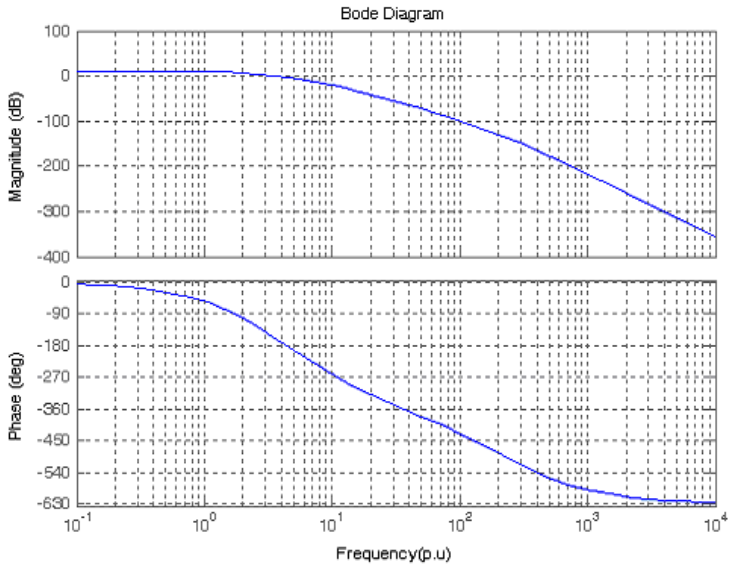

Figure 15: Bode diagram of the closed loop system.

In order to test the reliability of the derived dynamic models, a step disturbance of the load current was done and the outcomes of both the MATLAB numerical solution of the model equations and the PSIM simulation results for the same disturbance were matching. As a result, the dynamic model provided is robust enough to lean on.

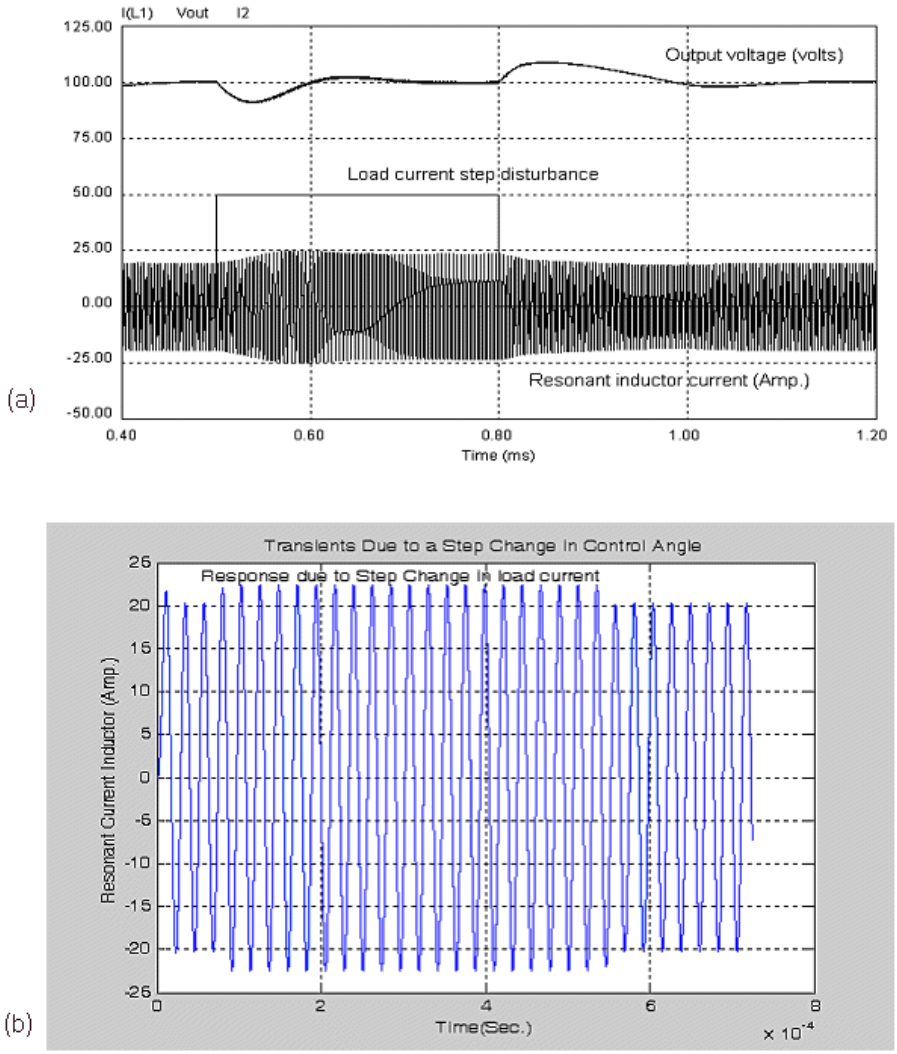

Figure 16: Comparison between PSIM (a) and MATLAB (b) simulations. Load current step disturbance (current scaled by 5 times).

5 Conclusions

In this paper an accurate sampled-data dynamic model for DC/DC self-sustained series-parallel resonant converter with a capacitive output filter has been presented to study the steady state, dynamic, and transient performance. The validity of the proposed modeling technique was proven through analytical, simulation, and experimental results. It has been shown in the paper that the series-parallel converter with capacitive output filter has better transient response than the converter with a inductive-capacitive output filter. The modeling technique presented in both parts will be useful in designing the resonant power supplies for a wide range of applications.

Appendix. Advantages of proposed (SSOC) controller over conventional variable frequency controller

In order to illustrate the advantages, we assume the real-time uncertainty of resonant elements such that:

$$\begin{aligned} 0.8L_{sno} \leq L_S \leq 1.2L_{sno} \\ 0.8C_{sno} \leq C_s \leq 1.2C_{sno} \end{aligned} \tag{A-1}$$

where (L_{sno}) and (C_{sno}) are the nominal values of (L_s) and (C_s), respectively. The voltage conversion ratio (M) of the converter, which ensures operation above the resonant frequency necessary for ZVS, was computed and shown in Figs.17 and 18 when equipped with both controllers each on a time.

The conventional variable frequency method will cause a reduction of (M) up to 62.5%, which means a loss of ZVS. The proposed controller will have a negligible effect on the maximum voltage conversion ratio (4.7%) to show its robustness.

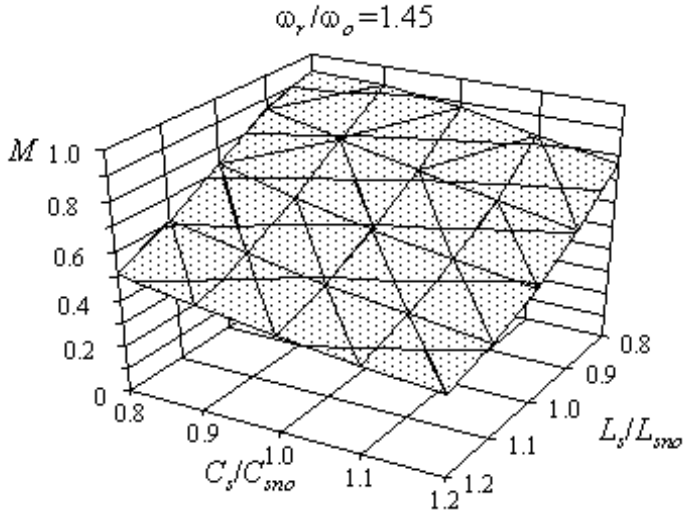

Figure 17: Maximum voltage conversion ratio for a conventional variable frequency control.

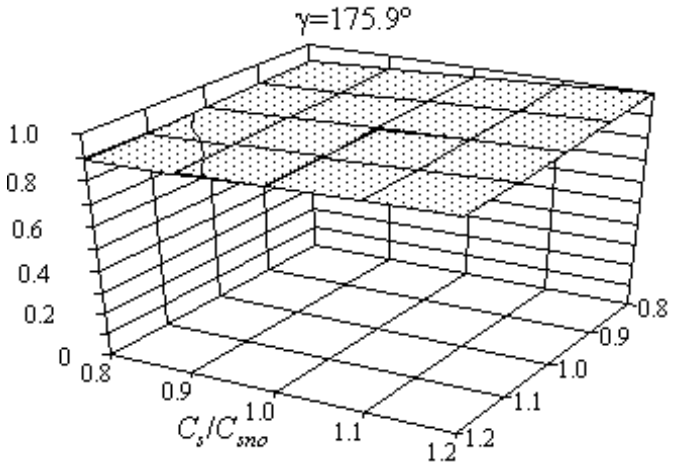

Figure 18: Maximum voltage conversion ratio for the proposed SSOC controller.

Nomenclature

f_o	Resonant tank frequency
i_s	Series resonant inductor current
i_p	Transformer primary side current
n_1/n_2	Isolating transformer turns ratio
Q_s	Resonant tank quality factor
S_t	Amplitude of saw-tooth signal
u_k	Input sources vector
v_g	Rated input voltage
v_{in}	Input voltage
v_o	Output voltage
V, v_{ab}	Resonant tank voltage
V_p	Reference voltage setting the amplitude of the saw-tooth signal (S_t)
v_p	Transformer primary voltage
v_{sec}	Transformer secondary voltage
v_{ca}	Control voltage
v_{co}	Voltage across output filter capacitor
v_{cs},v_s	Voltage across the series tank capacitor
v_{cp}	Voltage across the resonant tank parallel capacitor
w_k	Transition times vector at sample # (k)
x_k	State vector given at sample # (k)
x_s	Integral of the error value in the control loop
β	Series to parallel capacitance ratio
β'	Ratio of series resonant tank inductance to leakage inductance
ω_o	Resonant frequency
ω_{st}	Saw-tooth frequency
ω_s	Switching frequency
υ	Ratio of ω_{st} to ω_s
γ_b	Control angle

References

[1] H. Pinheiro, P.K. Jain, and G. Joós, IEEE Trans. on Power Electronics **14**, 803 (1999).

[2] C. Cuadros, C.Y. Lin, D. Boroyovich, R. Watson, P. Ribardiere, G. Skutt, and F.C. Lee, IEEE Applied Power Electronic Conference APEC'97, p.268 (1997).

[3] J. Bu, M. Sznaier, Z. Wang, and I. Batarseh, IEEE Trans. on Power Electronics **12**, 837 (1997).

[4] A.J. Forsyth, and Y.K.E. Ho, Proc. IEE Electr. Power Applications **144**, 131 (1997).

[5] K.M. Smedley, and S. Cuk, IEEE Tran. on Power Electronics **10**, 625 (1995).

[6] A.M. Stankovic, D.J. Perrault, and K. Sato, IEEE Power Electronics Specialist Conference, PESC'97, p.679 (1997).

[7] J.S. Lew and J.Lin, IEEE Trans. on Power Electronics **14**, 793 (1999).

[8] L. Rosseto, IEEE Power Electronics Specialist Conference, PESC'02, p.787 (2002).

[9] M.G. Kim, D.S. Lee, and M.J. Youn, IEEE Trans. on Industrial Electronics **38**, 173 (1991).

[10] S-C. Wong and A.D. Brown, IEEE Trans. on Power Electronics **10**, 605 (1995).

[11] H. Pinheiro, P.K. Jain, and G. Joós, IEEE Applied Power Electronic Conference APEC'97, p.993 (1997).